

β decay of nuclei around ^{90}Se : Search for signatures of a $N = 56$ subshell closure relevant to the r process

M. Quinn,^{1,2} A. Aprahamian,^{1,2} J. Pereira,^{3,4,*} R. Surman,^{2,5} O. Arndt,^{6,7} T. Baumann,³ A. Becerril,^{3,4,8} T. Elliot,^{3,4,8} A. Estrade,^{3,4,8} D. Galaviz,^{3,4} T. Ginter,³ M. Hausmann,⁹ S. Henrich,^{4,6,7} R. Kessler,^{4,6,7} K.-L. Kratz,^{7,10} G. Lorusso,^{3,4,8} P. F. Mantica,^{3,11} M. Matos,^{3,4} F. Montes,^{3,4} B. Pfeiffer,^{6,7} M. Portillo,⁹ H. Schatz,^{3,4,8} F. Schertz,^{4,6,7} L. Schnorrenberger,^{4,12} E. Smith,^{4,13} A. Stolz,³ W. B. Walters,¹⁴ and A. Wöhr^{1,2}

¹*Institute of Structure and Nuclear Astrophysics, University of Notre Dame, Notre Dame, Indiana, USA*

²*Joint Institute for Nuclear Astrophysics, University of Notre Dame, Notre Dame, Indiana, USA*

³*National Superconducting Cyclotron Laboratory, Michigan State University, East Lansing, Michigan, USA*

⁴*Joint Institute for Nuclear Astrophysics, Michigan State University, East Lansing, Michigan, USA*

⁵*Department of Physics and Astronomy, Union College, Schenectady, New York, USA*

⁶*Institut für Kernchemie, Universität Mainz, Mainz, Germany*

⁷*Virtuelles Institut für Struktur der Kerne and Nuklearer Astrophysik, Mainz, Germany*

⁸*Department of Physics and Astronomy, Michigan State University, East Lansing, Michigan, USA*

⁹*Facility for Rare Isotope Beams, Michigan State University, East Lansing, Michigan, USA*

¹⁰*Max Planck Institut für Chemie, Otto-Hahn-Institut, Mainz, Germany*

¹¹*Department of Chemistry, Michigan State University, East Lansing, Michigan, USA*

¹²*Institut für Kernphysik, TU Darmstadt, Darmstadt, Germany*

¹³*Department of Physics, Ohio State University, Columbus, Ohio, USA*

¹⁴*Department of Chemistry and Biochemistry, University of Maryland, College Park, Maryland, USA*

(Received 22 December 2011; revised manuscript received 31 January 2012; published 26 March 2012)

Background: Nuclear structure plays a significant role on the rapid neutron capture process (r process) since shapes evolve with the emergence of shells and subshells. There was some indication in neighboring nuclei that we might find examples of a new $N = 56$ subshell, which may give rise to a doubly magic $^{90}\text{Se}_{34}$ nucleus.

Purpose: β -decay half-lives of nuclei around ^{90}Se have been measured to determine if this nucleus has in fact a doubly magic character.

Method: The fragmentation of a ^{136}Xe beam at the National Superconducting Cyclotron Laboratory at Michigan State University was used to create a cocktail of nuclei in the $A = 90$ region.

Results: We have measured the half-lives of 22 nuclei near the r -process path in the $A = 90$ region. The half-lives of ^{88}As and ^{90}Se have been measured for the first time. The values were compared with theoretical predictions in the search for nuclear-deformation signatures of a $N = 56$ subshell, and its possible role in the emergence of a potential doubly magic ^{90}Se . The impact of such hypothesis on the synthesis of heavy nuclei, particularly in the production of Sr, Y, and Zr elements was investigated with a weak r -process network.

Conclusions: The new half-lives agree with results obtained from a standard global QRPA model used in r -process calculations, indicating that ^{90}Se has a quadrupole shape incompatible with a closed $N = 56$ subshell in this region. The impact of the measured ^{90}Se half-life in comparison with a former theoretical prediction associated with a spherical half-life on the weak r process is shown to be strong.

DOI: [10.1103/PhysRevC.85.035807](https://doi.org/10.1103/PhysRevC.85.035807)

PACS number(s): 23.40.-s, 21.10.Tg, 27.60.+j, 26.30.-k

I. INTRODUCTION

The rapid neutron-capture process (r process) is thought to be responsible for the origin of more than half of all nuclei beyond iron. While large uncertainties remain about the site of the r process and its exact location, it is thought to occur in environments with a high density of free neutrons. There are a number of astrophysical scenarios suggested as possible sites. These include the neutrino driven wind from core-collapse supernovae [1,2], two neutron-star mergers [3], γ -ray bursts [4], black-hole neutron-star mergers [5], relativistic jets associated with failed supernovae [5,6], or magnetohydrodynamic jets from supernovae [7]. The speed of

the r -process reaction sequence and the resulting abundances of the elements are significantly influenced by the β -decay properties of the nuclei involved, which are in turn directly related to the evolution of nuclear structure and deformation. In a recent measurement of the half-life of the doubly magic nucleus ^{78}Ni [8,9], it was shown that the persistence of the closed neutron and proton shells had a significant impact on the r -process abundance patterns, and theoretical predictions for the half-life were significantly longer than observed.

Recent observations of anomalously large abundances of stable Sr, Y, and Zr in some metal-poor stars, as compared to heavier neutron-capture elements [10], have brought about new questions regarding the r -process mechanism and possible site(s). Travaglio *et al.* [11] have interpreted these observations as evidence for a new neutron-capture light-element primary process (LEPP) responsible for the nucleosynthesis of Sr–Zr

*pereira@nscl.msu.edu

elements. However, the nature of this process remains unclear. Montes *et al.* [12] extracted an abundance pattern for the LEPP and demonstrated that it can be associated with different origins. Qian and Wasserburg suggested a charge-particle reaction process (CPR) [13], which could operate in neutrino-driven winds, even in instances when conditions for an r process are not achieved. Farouqi *et al.* [14,15] proposed that Sr–Zr elements can be primarily produced in the low-entropy expanding envelopes of core-collapse supernovae explosions through charge-particle and neutron-capture reactions.

The main motivation for the present work was to explore the possible existence of a new $N = 56$ subshell and its potential impact on the r process. Whereas the presence of a $N = 56$ subshell has been suggested for Rb–Zr elements, its persistence for lighter isotones needs further investigation. If the flow of r -process matter emerging from seed nuclei below Kr were trapped in an hypothetical $N = 56$ “ladder,” then the post freeze-out β decay of nuclei like ^{88}Ge , ^{89}As , and ^{90}Se would immediately translate into an enhanced production of stable Sr, Y, and Zr elements—exactly as it occurs at the $N = 82$, 126 shells, leading to the well-known $A \simeq 130$, 195 r -process abundance peaks, respectively.

We have measured the half-lives of 22 nuclei in the $A = 90$ region at the National Superconducting Cyclotron Laboratory (NSCL). The half-lives of ^{88}As and ^{90}Se are reported for the first time, and more precise measurements are presented for the remaining 20. The results are used as a nuclear-structure probe to study the deformation of the β -decay mother/daughter system, which in turn can provide first hints of the underlying shell structure (see for instance Refs. [9,16–20]).

In the following sections, the experimental setup and analysis techniques employed in the present work are presented. The results are then discussed in Sec. IV in the framework of the quasirandom phase approximation and the impact of the new measurements on the r process.

II. EXPERIMENT

A. Production and separation of nuclei

A primary ^{136}Xe beam was accelerated at the NSCL Coupled Cyclotron Facility [21] to 120 MeV/nucleon, with an average intensity of 1.5 pnA. Nuclei produced by the fragmentation of the primary beam in a 235 mg/cm^2 Be target were forward-emitted into the A1900 fragment separator [22]. The fragments of interest were separated in-flight using the $B\rho$ - ΔE - $B\rho$ technique [23]. The first stage of the separator was set to the magnetic rigidity corresponding to the peak of the momentum distribution of ^{88}As . An achromatic wedge at the intermediate (dispersive) focal plane was made by combining a BC400 plastic scintillator (I2SCI) (22.22 mg/cm^2 thickness) with a 22.51 mg/cm^2 Kapton wedge-foil. The magnets of the second half of the A1900 were set to a value corresponding to the magnetic rigidity of the ^{88}As fragment after passing through the wedge system. This provided a further filter to select a narrower group of elements. The resulting fragment cocktail was composed of $^{86-88}\text{As}$, $^{88-90}\text{Se}$, $^{90-93}\text{Br}$, $^{91-95}\text{Kr}$, $^{93-97}\text{Rb}$, $^{95-99}\text{Sr}$, $^{97-101}\text{Y}$, and $^{100-103}\text{Zr}$.

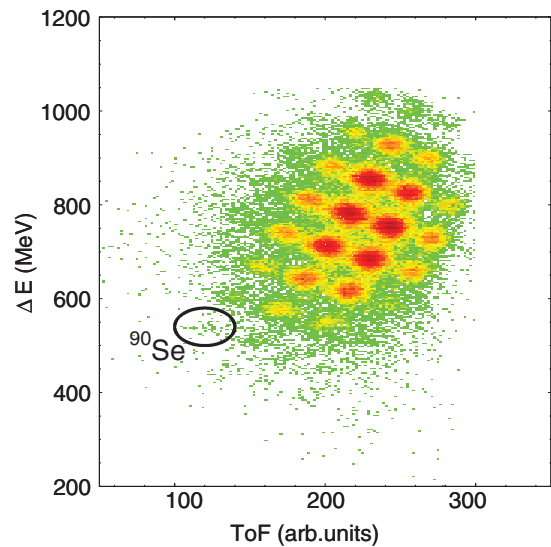


FIG. 1. (Color online) Particle-identification (PID) spectrum. The ToF of the transmitted nuclei is shown versus their energy-loss ΔE in the first Si PIN detector at the experiment station. (See text for details.)

The transmitted fragments were uniquely identified event-by-event, by combining their energy-loss measured in the first silicon PIN detector (PIN 1) of the implantation station, and the time-of-flight (ToF) measured between I2SCI and a scintillator located in the experimental area, 20 m downstream of the A1900 achromatic focal plane. To improve the ToF resolution, its dependence on the magnetic rigidity of the transmitted nuclei was corrected using the transversal position in the dispersive image plane measured with I2SCI. Figure 1 depicts the particle-identification spectrum (PID) recorded during the course of the experiment for fragments transported to the experimental station.

Besides the fragments of interest, the known μs isomers ^{98}Y and ^{99}Y were included in the A1900 setting. These nuclei were used as references to identify all the fragments transmitted in the same setting. The identification was done at the start of the experiment by implanting nuclei in a 4 mm-thick aluminum foil surrounded by three γ -ray detectors from the NSCL segmented germanium array (SeGA) [24]. A particle identification gated on the isomeric γ lines 121 keV, 171 keV, and 204 keV from ^{98}Y provided the reference for the identification of the nuclei in the cocktail. Once the particle identification was established, the implantation foil was removed to transmit particles to the implantation station for the remainder of the experiment.

Since the magnetic rigidity values of the μs isomers and the fragments of interest were significantly different, the A1900 was set up for the maximum possible $B\rho$ acceptance to allow for their simultaneous transmission. The $B\rho$ window included three primary-beam charge states $^{136}\text{Xe}^{+52}$, $^{136}\text{Xe}^{+51}$, and $^{136}\text{Xe}^{+50}$, with total intensities exceeding the maxima 1 MHz and 1 KHz tolerated by I2SCI and the Si PIN detectors, respectively. These contaminants were therefore blocked in the first image plane of the A1900 separator with a system

consisting of two slits on each side of the beam axis and a central tungsten finger.

B. The β -decay station

Nuclei transmitted through the A1900 were implanted in the NSCL Beta Counting System (BCS) [25]. The BCS was composed by a stack of four silicon PIN detectors (PIN 1–4) of total thickness $2569\ \mu\text{m}$, a $979\ \mu\text{m}$ -thick 40×40 doubly sided silicon strip detector (DSSD) (40 front-side perpendicular to 40 back-side strips) and a $988\ \mu\text{m}$ -thick 16-strip single-sided Si strip detector (SSSD). A 10 mm-thick Ge crystal downstream of the SSSD was used for light-particle veto purposes. Each PIN detector was connected to a preamplifier with an energy range of 10 GeV. The DSSD strips were connected to dual-gain preamplifiers with ranges equivalent to 3 GeV and 100 MeV, so that signals from implantations and β decays could be processed. The 16 SSSD strips were connected to a 16-channel high-gain preamplifier to distinguish β -decay particles from other particles that produced low-energy signals in the DSSD. The high-gain signals from the DSSD and SSSD preamplifiers were further processed by shaper/discriminator modules designed at Washington University, St. Louis, and manufactured by Pico Systems [26]. These modules include shaper and discriminator circuits sharing the same input, and provide independent logic and analogic output signals. The gain of each channel was adjusted in the beginning of the experiment to energy-match the signals from each DSSD strips generated by a ^{228}Th α source. Independent CFD thresholds were adjusted for each DSSD strip with a ^{90}Sr β -decay source. This source was also used to define two thresholds for each SSSD strip, one (th_1) above the noise peak, and the other (th_2) just above the β -decay energy region. Thresholds for each PIN detectors were set on-line using the energy spectra recorded during the experiment.

The DSSD and the four PIN detectors were energy-calibrated by comparing the signals from different transmitted nuclei with the values calculated with the LISE program [27], using the Ziegler energy-loss formulation [28]. A dedicated unwedged setting of the A1900, transmitting a large number of different fragments, was used in the beginning of the experiment to cover as broad an energy range as possible. The total kinetic energy (TKE) of each transmitted ion was determined by summing the calibrated energy signals from the four PIN detectors and the DSSD. The TKE was used to determine the charge states of the transmitted ions. Thus, fully stripped nuclei could be separated from charge-state contaminants—mostly hydrogen-like ions with mass numbers $A - 2$ and $A - 3$, and helium-like ions with mass number $A - 5$ —with similar ΔE and ToF values. An example of the charge-state separation based on TKE is shown in Fig. 2 for Sr isotopes. For each isotope, the high-TKE peak arises from the fully stripped species, whereas the medium- and lowest-TKE peaks correspond to the hydrogen-like and helium-like contaminants, respectively. As can be seen, nearly all the charge-state contaminants were implanted in the last PIN. On the other hand, there was a fraction of fully stripped nuclei of interest that passed through the DSSD and were thus implanted

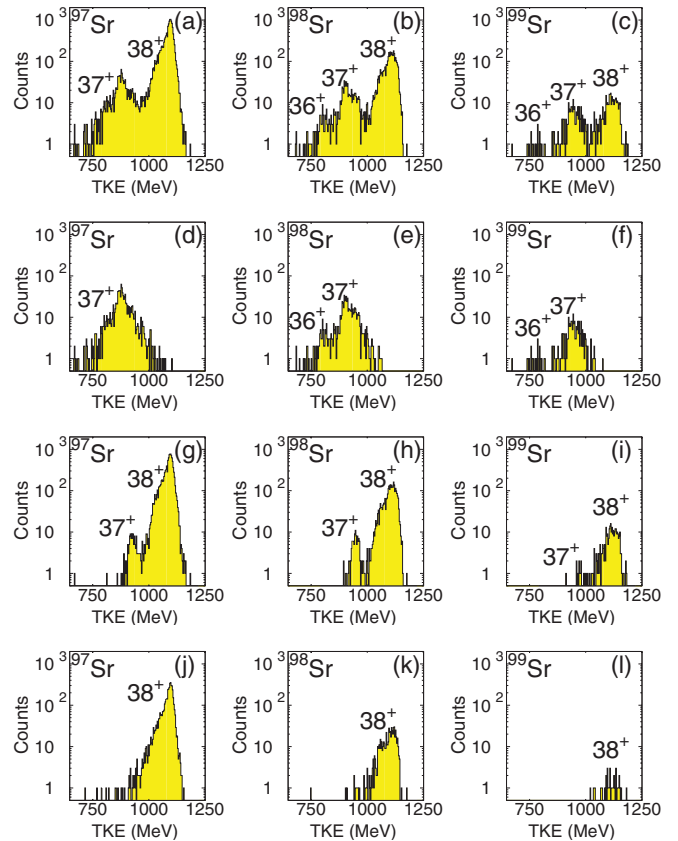


FIG. 2. (Color online) Measured total-kinetic-energy (TKE) distributions for Sr isotopes, including fully stripped, hydrogen-like, and helium-like ions (38^+ , 37^+ , and 36^+ , respectively). (a), (b), and (c) correspond to all nuclei detected with the first Si-stack detector (PIN 1); (d), (e), and (f) depict nuclei that were implanted in the most downstream Si-stack detector (PIN 4); (g), (h), and (i) represent nuclei that were implanted in the doubly sided Si detector (DSSD); and (j), (k), and (l) correspond to all nuclei that punched through the (DSSD) and were implanted in the single-sided Si detector (SSSD).

in the SSSD. The fraction of these lost events was negligible for the lightest, neutron-rich nuclei of interest.

III. DATA ANALYSIS

A. Identification of β decays

An implantation event was defined as a signal in the first PIN detector in coincidence with low-gain output signals from at least one strip on each side of the DSSD, and in anticoincidence with signals from SSSD above threshold th_2 (see Sec. II B). Decay-like events were defined by a high-gain output signal from at least one strip on each side of the DSSD, in anticoincidence with signals from any PIN detector, SSSD above th_2 , and Ge overflows generated by light particles. For each implantation event, the strip location on each side of the DSSD, defining the implanted pixel, was calculated as the average between all the strips weighted by their respective energy-signal amplitude. The implanted pixel

and time, registered by a continuously counting 50 MHz clock, were recorded for all implantation events. Subsequent decay-like events occurring in the same or nearest neighbor pixels (defining a cluster of nine pixels) within a given correlation-time window t_c were associated with the previous implantation, and their times and pixels recorded. Different values of t_c were used in the analysis following the criterion $t_c \simeq 5 \times T_{1/2}$, where $T_{1/2}$ was the expected half-life of the nucleus of interest. If a decay-like event was time correlated with more than one implantation measured in the same nine-pixel cluster (back-to-back implants), then all the events within the sequence were rejected. Data were taken in 1-hr runs over a total running time of 140 hr.

Several sources contributed to the β -decay background. The most important were light particles that did not lead to overflows in the Ge detector and had energies in SSSD below th_2 and above th_1 (i.e., in the β -like event region); real β decays from longer-lived nuclei implanted in the same pixel; and electronic noise signals above the thresholds. The number of β -like events in each nine-pixel cluster, occurring at a time t_b after a preceding implantation was recorded for each 1-hr run time to quantify the β -decay background. The optimum value of t_b was determined from an analysis of the total background rate R_b as a function of t_b . If t_b was too short, R_b included background events and real correlated β decays. As t_b increased, the number of real correlated β decays contributing to R_b was lower, and R_b decreased with t_b . Beyond a given value of t_b , no correlated β decay were included and R_b remained constant. The optimum value was found at $t_b = 40$ s. The background rate of each nine-pixel cluster and run was used to compute the total background rate of each isotope. An average background rate, among the different nuclei analyzed, of about 0.01 s^{-1} was found with a variance within the statistical error. The statistical error derived from the number of background events recorded in each DSSD cluster and run was about 8%. The number of background events B_β associated with a given isotope was calculated by multiplying its background rate by the number of implants and the correlation time t_c .

B. β -decay half-lives

Up to three correlated β -decay events were accepted for each implantation, defining a β -decay chain. Possible members of these chains included the β decay of the daughter and grand-daughter; the β decay of the daughter and grand-daughter generated by β -delayed neutron emission from the implanted nucleus; and the β decay of the grand-daughter following the β -delayed two-neutron emission from the β -decay daughter. For each implantation, the decay times t_i (with $i = 1, 2, \text{ or } 3$) of the three β -decay chain members were recorded along with the background rate in the corresponding cluster. All the decay chains of a given nucleus were analyzed using the maximum likelihood method (MLH) described in Ref. [16]. Additional input quantities required in this method included the β -decay detection efficiency ϵ_β , and the half-lives and β -delayed neutron-emission probabilities of all the members of the decay chain (taken from Ref. [29]).

The β -decay detection efficiency ϵ_β was calculated as the ratio of the number of detected β decays (N_β) from the mother nucleus to the number of implantations. In order to determine N_β , a multiparameter decay function was fitted by least-squares to the decay-curve histograms recorded for some nuclei. This fit function was derived from the Bateman equations [30]. It included, as input parameters, the half-lives and P_n values of all the descendant members of the corresponding decay chain, and a constant background. The value of N_β was calculated as $N_\beta = N_0/(\lambda_1 \Delta t)$, where Δt is the size of the bin histogram. The decay constant λ_1 and the initial number of decaying nuclei N_0 were obtained from the fit. As discussed in Ref. [16], the total number of events per bin in the decay-curve histogram must be sufficiently high (i.e., above $\simeq 10$) for the least-squares method to be statistically justified. The resulting efficiency was nearly constant among all the nuclei considered. A weighted average efficiency (29 ± 5 %) was used in the MLH fits.

The sources of error in the half-lives stem from uncertainties in the input parameters used in the fits. These parameters were the background rate, the decay parameters of the descendant nuclei, and the decay efficiency ϵ_β (only for half-lives determined using the MLH method). The average contribution to the total systematic error was 2.9% from background, 0.5% from decay parameters, and 5.2% from efficiency (for the MLH method). In some cases, the contribution of the efficiency uncertainty gave rise to a systematic error in MLH significantly higher than the value obtained from the least-squares method. The statistical error in the MLH method was calculated using the method proposed by Brüche [31].

IV. RESULTS AND DISCUSSION

The deduced β -decay half-lives are listed in Table I, along with their systematic and statistical errors. The statistical error was in most cases significantly larger than the systematic one. For the sake of completeness, the half-lives obtained from least-squares fits of the decay curves for those cases with sufficient statistics are listed as well. The measured half-lives for different isotopic chains are shown in Fig. 3 (filled circles), where only statistical errors are included. The present data agree with previous measurements (open circles) within $1-\sigma$ uncertainty. An exception is ^{88}Se whose half-life reported here is significantly lower than the value found in the literature.

As expected on the basis of the Q_β evolution, the half-lives systematics follow a decreasing trend with increasing neutron number. The discontinuity in the half-lives systematics of ^{38}Sr isotopes, with an abrupt drop at ^{97}Sr , arises from the presence of high-energy $1/2^-$ states in $^{97}\text{Y}_{58}$ (probably from $p_{1/2}$ configurations) which absorb most of the β -decay strength S_β via allowed transitions from the $1/2^-$ ground state of ^{97}Sr . Such allowed transitions are not possible from the $^{98}\text{Sr}_{60}$ ground state 0^+ , which decays via forbidden transitions into a daughter's spectrum dominated by negative-parity states. Such states involve the coupling of the $p_{1/2}$ proton orbital with $s_{1/2}$, $d_{3/2}$, and/or $g_{7/2}$ neutron orbitals, coexisting with negative-parity states [32].

TABLE I. Total number of implantations, number of correlated decay sequences N , and experimental β -decay half-lives obtained from the maximum likelihood method (MLH) and least-squares fits (Least squares). Systematic and statistical errors are given by the first and second numbers following the half-life values. The results are compared with known half-life values [29].

Isotope	Implantations	N	Half-life (ms)		
			This work MLH	This work Least squares	Literature
^{87}As	27	12	$1450(550)^{+3900}_{-1100}$		560(80)
^{88}As	16	8	$200(5)^{+200}_{-90}$		
^{88}Se	144	74	$650(35)^{+175}_{-140}$		1530(60)
^{89}Se	180	90	$345(20)^{+95}_{-75}$		410(40)
^{90}Se	70	30	$195(7)^{+95}_{-65}$		
^{90}Br	869	369	$1850(110)^{+190}_{-170}$	2085(25)(230)	1910(10)
^{91}Br	1158	531	$615(35)^{+60}_{-50}$	495(30)(40)	541(5)
^{92}Br	309	161	$290(15)^{+70}_{-55}$		343(15)
^{93}Br	45	20	$69(1)^{+40}_{-25}$		102(10)
^{93}Kr	1661	831	$1040(65)^{+80}_{-75}$	1245(30)(70)	1290(10)
^{94}Kr	881	480	$282(10)^{+28}_{-25}$	275(1)(27)	212(5)
^{95}Kr	152	68	$250(10)^{+75}_{-55}$		114(3)
^{95}Rb	7587	3253	410(20)(25)	412(1)(13)	378(1)
^{96}Rb	1972	1904	220(8)(17)	212(6)(16)	203(3)
^{97}Rb	291	164	$208(5)^{+42}_{-36}$		169(1)
^{96}Sr	10520	5385	940(45)(60)	950(25)(25)	1070(10)
^{97}Sr	9763	5082	450(25)(30)	456(5)(13)	429(5)
^{98}Sr	2545	1377	640(20)(35)	577(1)(30)	653(2)
^{99}Sr	231	131	$420(20)^{+115}_{-90}$		269(1)
^{99}Y	6061	3394	1355(65)(85)	1400(15)(70)	1470(7)
^{100}Y	1699	878	840(55)(80)	845(45)(60)	735(7)
^{101}Y	239	117	$480(30)^{+140}_{-110}$		450(20)

The presence of an $N = 56$ subshell gap in the region below Zr has motivated numerous studies with contradictory outcomes. The semi-magic character of $N = 56$ for $Z = 37\text{--}42$ is supported on the basis of the 2^+_1 -energy ($E2^+_1$) systematics. As for $^{92}\text{Kr}_{56}$, the smooth evolution of low-energy

states in ^{93}Kr as compared with ^{95}Sr was interpreted by Lhersonneau *et al.* [33] as a signature of the persistence of the $N = 56$ subshell for the Kr isotopes. On the other hand, the vanishing of this subshell for ^{92}Kr was suggested by Delahaye *et al.* [34], based on their mass measurement

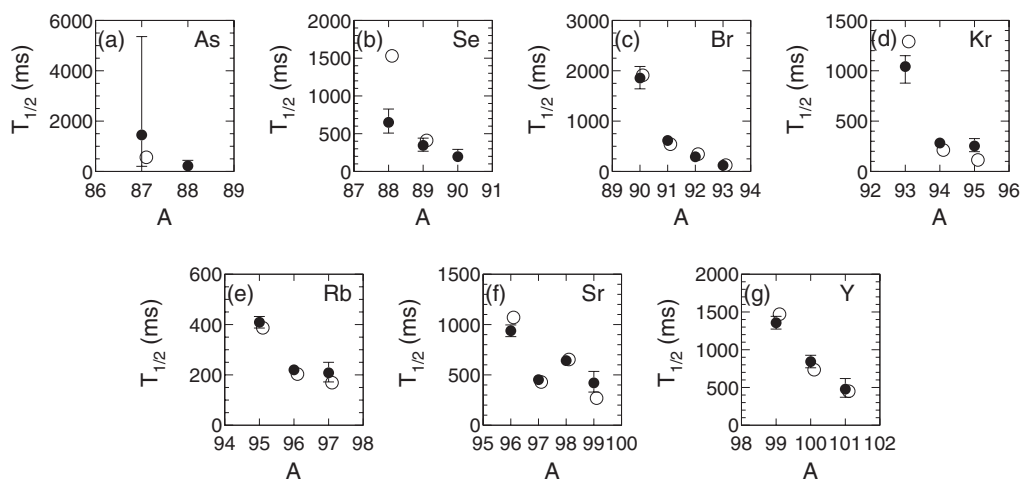


FIG. 3. β -decay half-lives obtained in this work from the maximum likelihood method for the As, Se, Br, Kr, Rb, Sr, and Y isotopes (filled circles), compared with results from previous experiments [29] (open circles); the latter were shifted slightly in A for visual clarity.

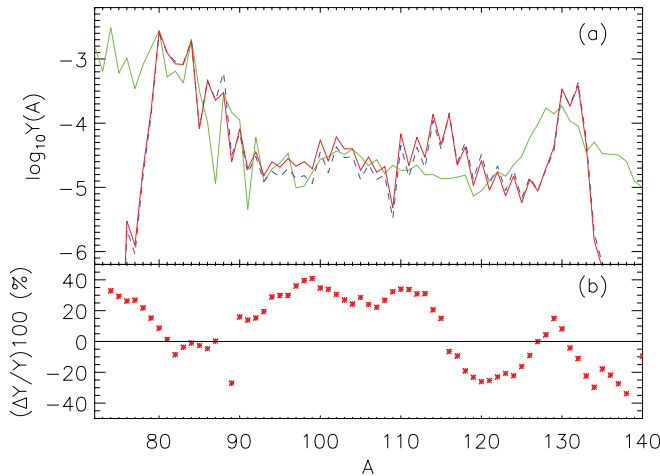


FIG. 4. (Color online) A comparison of the r -process abundances resulting from a simulation using the new measured half-life of ^{90}Se (solid red line) and the value calculated with Möller's QRPA model for a spherical ^{90}Se (blue dashed line). (a) Outputs of both simulations shown against the scaled solar abundances (green thin line) [38]. (b) Relative difference between the two calculated abundance patterns. The r -process simulation uses constant temperature conditions with $T = 1.43 \times 10^9$ K and initial neutron density of $N_n = 5.0 \times 10^{22}/\text{cm}^3$. All three curves are normalized to each other at $A = 80$.

results. This conclusion is supported by the large quadrupole collectivity deduced from the $B(E2; 0^+ \rightarrow 2^+)$ measured at REX-ISOLDE [35] for this isotope. In the light of these results, the unexpectedly high 2_1^+ energy measured for $^{88}\text{Se}_{54}$ by Jones *et al.* [36] has special significance. Such a sudden increase of the $E2_1^+$ energies for the $N = 54$ isotone systematics could be a harbinger of an even higher energy in $^{90}\text{Se}_{56}$, compatible with a spherical shape. The monopole shift induced by the complete filling of the $d_{5/2}$ neutron orbital for the $N = 56$ isotones might push the $\pi f_{5/2}$ orbital down, and the $\pi p_{3/2}$ orbital up in energy, creating a $Z = 34$ subshell. Such a scenario would explain the large value of $E2_1^+$ measured for $^{88}\text{Se}_{54}$. In addition, due to the complete filling of the $\nu d_{5/2}$ orbital for $N = 56$, $^{90}\text{Se}_{56}$ would emerge as a new doubly magic nucleus. A similar monopole shift has been reported for the proton orbitals in odd-mass ^{29}Cu isotopes. There, the $5/2^-$ ground state assigned to $^{75}\text{Cu}_{46}$ [37] is an indication of an inversion of the $\pi p_{3/2}$ ground state and $\pi f_{5/2}$ excited state of $^{69}\text{Cu}_{40}$, ascribed to the addition of neutrons to the $g_{9/2}$ orbital.

A doubly magic $^{90}\text{Se}_{56}$ nucleus would have a very different impact on the r -process abundance pattern than a deformed shape. In the top panel of Fig. 4, the observed solar r -process abundances (green thin solid line) are compared with results obtained from network calculations [39] with astrophysical conditions for a weak r process (temperature $T = 1.43 \times 10^9$ K and initial neutron density $N_n = 5.0 \times 10^{22}/\text{cm}^3$). The half-life and P_n values of the nuclei included in the network were taken from Ref. [40] with the exception of ^{90}Se . For this nucleus, we used the new measured half-life (red solid line), and the value calculated with Möller's QRPA model assuming a spherical shape consistent with a doubly-magic

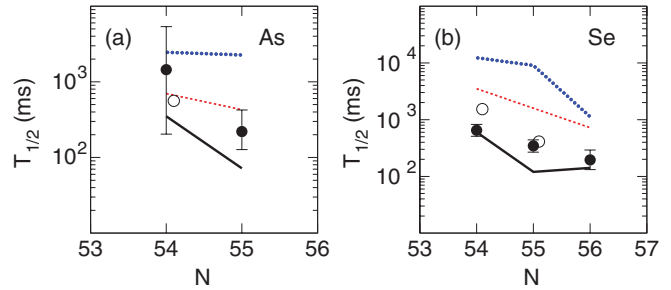


FIG. 5. (Color online) β -decay half-lives obtained from the maximum likelihood method for As (a) and Se (b) isotopes (filled dots), compared with results from calculations by Möller *et al.* QRPA97 [40] (solid black line) and QRPA03 [43] (dashed red line), both of which use the nuclear deformation parameters from FRDM [44]. The dotted blue line corresponds to QRPA sph, which was calculated assuming spherical nuclear shapes. The half-lives measured in previous experiments [29] are shown by open circles. (See text for details.)

^{90}Se . The percentage differences between both calculations are shown in linear scale in the bottom panel. It is remarkable how the half-life of a hypothetically spherical doubly magic ^{90}Se induces variations in the calculated abundances of more than 40% in the $A = 70$ – 140 region. Moreover, after the neutron freeze-out, the large amount of matter accumulated in this pseudo-waiting-point nucleus decays through a series of β decays that includes the emission of up to two neutrons. As seen in Fig. 4, the net result is an overproduction of the stable ^{88}Sr nucleus. (Note that for $A = 88$ the percentage difference is out of scale in the bottom panel of the figure.)

The half-lives deduced for ^{33}As and ^{34}Se isotopes in the present work are compared in Fig. 5 to values obtained from three different calculations based on the quasirandom phase approximation (QRPA) [41,42]. In the first (QRPA97 [40]) and second (QRPA03 [43]) calculations (solid and dashed lines, respectively), the nuclear-deformation parameters were determined using the Finite-range droplet model (FRDM) of Möller *et al.* [44]. In addition, QRPA03 includes first-forbidden transition rates obtained from the statistical gross theory [45,46]. The third calculation (QRPA sph) (Fig. 5, dotted blue line) was done using QRPA03, assuming spherical nuclear shapes for both, the mother and the daughter isobars.

In the case of $^{87}\text{As}_{54}$, the three calculations agree with the adopted half-life within $1-\sigma$ error. However, the more precise half-life for this nucleus from the ENSDF database [29] (obtained by statistical evaluation among three independent experiments) and the new half-life for ^{88}As are only compatible with QRPA03.

Similar results were obtained for the half-lives of the ^{34}Se isotopes. The half-lives calculated with QRPA sph are too high presumably due to the dominance of forbidden transitions between levels of opposite parity, involving $f_{5/2}$, $p_{3/2}$, $p_{1/2}$ proton orbitals, and $d_{5/2}$, $g_{7/2}$, $s_{1/2}$, $d_{3/2}$ neutron orbitals. QRPA97 provides the best agreement with the new measured half-life of ^{90}Se , implying that this nucleus is not doubly magic but in fact, deformed. According to Ref. [40], ^{90}Br is the first neutron-rich Br isotope in which the ground state is defined by the coupling of the $1/2^+$ deformation-driving state, from the

$\pi g_{9/2}$ orbital, with the $3/2^+$ state from the $\nu d_{5/2}$ orbital. In this context, the new half-life of ^{90}Se obtained here rules out the possibility of a spherical waiting point that would contribute to the overproduction of stable Sr, Y, and Zr isotopes observed in some metal-poor stars [10].

V. SUMMARY

The β -decay half-lives of ^{33}As , ^{34}Se , ^{35}Br , ^{36}Kr , ^{37}Rb , ^{38}Sr , and ^{39}Y isotopes around $N = 56$ were measured at the National Superconducting Cyclotron Laboratory. New half-lives are reported for $^{88}\text{As}_{55}$ and $^{90}\text{Se}_{56}$ for the first time.

The β decays from the nuclei of interest were observed with the β counting system. The half-lives were deduced using the maximum likelihood method and, where statistics were sufficient, least-squares fits of decay curves. Agreement between both analyzes brings confidence to the results. For most of the cases, the data agree with previous measurements.

The structure of $N = 56$ isotones in this region was investigated by comparing the measured half-lives with QRPA calculations. The deformed intruder states from $\pi g_{9/2}$ and

$\nu h_{11/2}$ orbitals play a crucial role creating allowed transitions that compensate the slow forbidden transitions dominating the β decay of a spherical ^{90}Se .

No evidence was found for a $N = 56$ subshell closure in $^{90}\text{Se}_{56}$, let alone the emergence of a new $Z = 34$ semimagic number due to the monopole interaction between $\pi f_{5/2}$ and $\nu d_{5/2}$ orbitals. Nevertheless, given the gross nature of β -decay half-lives as a nuclear-structure probe, more precise spectroscopic studies of $^{90}\text{Se}_{56}$ are needed.

ACKNOWLEDGMENTS

The authors wish to thank the NSCL operations staff and R. Fox for their help in the preparation and running of the experiment, as well as Peter Möller for providing his calculated half-lives for spherical nuclear shapes. This work was supported in part by the Joint Institute for Nuclear Astrophysics (JINA) under NSF Grant Nos. PHY-02-16783, PHY 08-22648, the Institute of Nuclear Structure and Astrophysics under NSF grant no. PHY-07-58100, and the National Superconducting Cyclotron Laboratory (NSCL) under NSF Grant Nos. PHY-01-10253 and PHY-06-06007.

-
- [1] S. E. Woosley, J. R. Wilson, G. J. Mathews, G. J. Hoffman, and B. S. Meyer, *Astrophys. J.* **433**, 229 (1994).
- [2] K. Takahashi, J. Witt, and H.-Th. Janka, *Astron. Astrophys.* **286**, 857 (1994).
- [3] C. Freiburghaus, S. Rosswog, and F.-K. Thielemann, *Astrophys. J.* **525**, L121 (1999).
- [4] R. Surman, G. C. McLaughlin, and W. R. Hix, in *Proceedings of Science*, PoS (NIC-IX), 35 (2006); [http://pos.sissa.it/archive/conferences/028/035/NIC-IX_035.pdf].
- [5] R. Surman, G. C. McLaughlin, M. Ruffert, H.-Th. Janka, and W. R. Hix, *Astrophys. J.* **679**, L117 (2008).
- [6] S.-I. Fujimoto, K. Kotake, S. Yamada, M.-A. Hashimoto, and K. Sato, *Astrophys. J.* **644**, 1040 (2006).
- [7] N. Nishimura, M.-A. Hashimoto, S.-I. Fujimoto, K. Kotake, and S. Yamada, *AIP Conf. Proc.* **847**, 452 (2006).
- [8] P. T. Hosmer, H. Schatz, A. Aprahamian, O. Arndt, R. R. C. Clement, A. Estrade, K.-L. Kratz, S. N. Liddick, P. F. Mantica, W. F. Mueller, F. Montes, A. C. Morton, M. Ouellette, E. Pellegrini, B. Pfeiffer, P. Reeder, P. Santi, M. Steiner, A. Stolz, B. E. Tomlin, W. B. Walters, and A. Wöhr, *Phys. Rev. Lett.* **94**, 112501 (2005).
- [9] P. T. Hosmer, H. Schatz, A. Aprahamian, O. Arndt, R. R. C. Clement, A. Estrade, K. Farouqi, K.-L. Kratz, S. N. Liddick, A. F. Lisetskiy, P. F. Mantica, P. Möller, W. F. Mueller, F. Montes, A. C. Morton, M. Ouellette, E. Pellegrini, J. Pereira, B. Pfeiffer, P. Reeder, P. Santi, M. Steiner, A. Stolz, B. E. Tomlin, W. B. Walters, and A. Wöhr, *Phys. Rev. C* **82**, 025806 (2010).
- [10] S. Honda, W. Aoki, Y. Ishimaru, S. Wanajo, and S. G. Ryan, *Astrophys. J.* **643**, 1180 (2006).
- [11] C. Travaglio, R. Gallino, E. Arnone, J. J. Cowan, F. Jordan, and C. Sneden, *Astrophys. J.* **601**, 864 (2004).
- [12] F. Montes, T. C. Beers, J. J. Cowan, T. Elliot, K. Farouqi, R. Gallino, M. Heil, K.-L. Kratz, B. Pfeiffer, M. Pignatari, and H. Schatz, *Astrophys. J.* **671**, 1685 (2007).
- [13] Y.-Z. Qian and G. J. Wasserburg, *Phys. Rep.* **442**, 237 (2007).
- [14] F. Farouqi, K.-L. Kratz, L. I. Mashonkina, B. Pfeiffer, J. J. Cowan, F.-K. Thielemann, and J. W. Truran, *Astrophys. J. Lett.* **694**, L49 (2009).
- [15] K. L. Kratz, F. Farouqi, L. I. Mashonkina, and B. Pfeiffer, *New Astron. Rev.* **52**, 390 (2008).
- [16] J. Pereira, S. Hennrich, A. Aprahamian, O. Arndt, A. Becerril, T. Elliot, A. Estrade, D. Galaviz, R. Kessler, K.-L. Kratz, G. Lorusso, P. F. Mantica, M. Matos, P. Möller, F. Montes, B. Pfeiffer, H. Schatz, F. Schertz, L. Schnorrenberger, E. Smith, A. Stolz, M. Quinn, W. B. Walters, and A. Wöhr, *Phys. Rev. C* **79**, 035806 (2009).
- [17] P. Sarriguren and J. Pereira, *Phys. Rev. C* **81**, 064314 (2010).
- [18] K.-L. Kratz, *Nucl. Phys. A* **417**, 447 (1984).
- [19] T. Mehren, B. Pfeiffer, S. Schoedder, K.-L. Kratz, M. Huhta, P. Dendooven, A. Honkanen, G. Lhersonneau, M. Oinonen, J.-M. Parmonen, H. Penttilä, A. Popov, V. Rubchenya, and J. Äystö, *Phys. Rev. Lett.* **77**, 458 (1996).
- [20] O. Sorlin, D. Guillemaud-Mueller, A. C. Mueller, V. Borrel, S. Dogny, F. Pougheon, K.-L. Kratz, H. Gabelmann, B. Pfeiffer, A. Wöhr, W. Ziegert, Y. E. Penionzhkevich, S. M. Lukyanov, V. S. Salamatina, R. Anne, C. Borcea, L. K. Fifield, M. Lewitowicz, M. G. Saint-Laurent, D. Bazin, C. Détraz, F.-K. Thielemann, and W. Hillebrandt, *Phys. Rev. C* **47**, 2941 (1993).
- [21] The K500@K1200, A Coupled Cyclotron Facility at the National Superconducting Cyclotron Laboratory, NSCL Report No. MSUCL-939, July, 1994 (unpublished).
- [22] D. J. Morrissey, B. M. Sherrill, M. Steiner, A. Stolz, and I. Wiedenhoever, *Nucl. Instrum. Methods Phys. Res. B* **204**, 90 (2003).
- [23] K.-H. Schmidt, E. Hanelt, H. Geissel, G. Münzenberg, and J.-P. Dufour, *Nucl. Instrum. Methods Phys. Res. A* **260**, 287 (1987).

- [24] W. F. Mueller, J. A. Church, T. Glasmacher, D. Gutknecht, G. Hackman, P. G. Hansen, Z. Hu, K. L. Miller, and P. Quirin, *Nucl. Instrum. Methods Phys. Res. A* **466**, 492 (2001).
- [25] J. I. Prisciandaro, A. C. Morton, and P. F. Mantica, *Nucl. Instrum. Methods Phys. Res. A* **505**, 140 (2003).
- [26] J. Elson (private communication) [<http://pico-systems.com>].
- [27] D. Bazin, O. B. Tarasov, M. Lewitowicz, and O. Sorlin, *Nucl. Instrum. Methods Phys. Res. A* **482**, 307 (2002).
- [28] J. F. Ziegler, J. P. Biersack, and U. Littmar, in *Stopping and Ranges of Ions in Matter*, edited by J. F. Ziegler, Vol. 1 (Pergamon, New York, 1985).
- [29] Evaluated Nuclear Structure Data File (ENSDF), April 21, 2008.
- [30] J. Cetnar, *Ann. of Nucl. En.* **33**, 640 (2006).
- [31] W. Bröchle, *Radiochim. Acta* **91**, 71 (2003).
- [32] S. Brant, V. Paar, G. Lhersonneau, O. W. B. Schult, H. Seyfarth, and K. Systemich, *Z. Phys. A* **334**, 517 (1989).
- [33] G. Lhersonneau, A. Wöhr, B. Pfeiffer, K.-L. Kratz, and the ISOLDE Collaboration, *Phys. Rev. C* **63**, 034316 (2001).
- [34] P. Delahaye, G. Audi, K. Blaum, F. Carrel, S. George, F. Herfurth, A. Herlert, A. Kellerbauer, H. J. Kluge, D. Lunney, L. Schweikhard, and C. Yazidjian, *Phys. Rev. C* **74**, 034331 (2006).
- [35] D. Müller *et al.*, in *13th International Symposium on Gamma-Ray Spectroscopy and Related Topics*, edited by J. Jolie, A. Zilges, N. Warr, and A. Blazhev (American Institute of Physics, Cologne, Germany, 2009), Vol. CP1090, p. 587.
- [36] E. F. Jones, P. M. Gore, J. H. Hamilton, A. V. Ramayya, J. K. Hwang, A. P. deLima, S. J. Zhu, C. J. Beyer, Y. X. Luo, W. Ma, J. O. Rasmussen, I. Y. Lee, S. C. Wu, T. N. Ginter, M. Stoyer, J. D. Cole, A. V. Daniel, G. M. Ter-Akopian, and R. Donangelo, *Phys. Rev.* **73**, 017301 (2006).
- [37] K. T. Flanagan, P. Vingerhoets, M. Avgoulea, J. Billowes, M. L. Bissell, K. Blaum, B. Cheal, M. DeRydt, V. N. Fedosseev, D. H. Forest, Ch. Geppert, U. Köster, M. Kowalska, J. Krämer, K. L. Kratz, A. Krieger, E. Mané, B. A. Marsh, T. Materna, L. Mathieu, P. L. Molkanov, R. Neugart, G. Neyens, W. Nörtershäuser, M. D. Seliverstov, O. Serot, M. Schug, M. A. Sjoedin, J. R. Stone, N. J. Stone, H. H. Stroke, G. Tungate, D. T. Yordanov, and Yu. M. Volkov, *Phys. Rev. Lett.* **103**, 142501 (2009).
- [38] C. Sneden, J. J. Cowan, and R. Gallino, *Annu. Rev. Astron. Astrophys.* **46**, 241 (2008).
- [39] R. Surman and J. Engel, *Phys. Rev. C* **64**, 035801 (2001).
- [40] P. Möller, J. R. Nix, and K.-L. Kratz, *At. Data Nucl. Data Tables* **66**, 131 (1997).
- [41] J. Krumlinde and P. Möller, *Nucl. Phys. A* **417**, 419 (1984).
- [42] P. Möller and J. Randrup, *Nucl. Phys. A* **514**, 1 (1990).
- [43] P. Möller, B. Pfeiffer, and K.-L. Kratz, *Phys. Rev. C* **67**, 055802 (2003).
- [44] P. Möller, J. R. Nix, W. D. Myers, and W. J. Swiatecki, *At. Data Nucl. Data Tables* **59**, 185 (1995).
- [45] K. Takahashi, *Prog. Theor. Phys.* **47**, 1500 (1972).
- [46] K. Takahashi, M. Yamada, and T. Kondoh, *At. Data Nucl. Data Tables* **12**, 101 (1973).